Laboratory and field performance of a 6000 dbar-rated CTD: the RBR*argo*|deep6k

Mathieu Dever
RBR
Ottawa, CANADA
Woods Hole Oceanographic Inst.
Woods Hole, MA, USA
mathieu.dever@rbr-global.com
0000-0002-4292-6368

Jean-Michel Leconte
RBR
Ottawa, CANADA
jean-michel.leconte@rbr-global.com

Greg Johnson
RBR
Ottawa, CANADA
greg.johnson@rbr-global.com

***Abstract*—The Deep Argo program's initiative to explore the deepest regions of the world's oceans up to 6000 m necessitates the deployment of robust, precise, and stable measurements of pressure, temperature, and salinity. This study evaluates the performance of the RBR*argo*|deep6k CTD, designed by RBR for deep-ocean applications, characterized through laboratory experiments and validated in-situ. The main challenges addressed are the errors generated by the compressibility of conductivity cell at high pressure, as well as its thermal inertia during profiling, affecting conductivity measurements. The results indicate that the compressibility calibration derived in the calibration facilities by the manufacturer performs as expected when deployed in the ocean. It also demonstrates that the corrective algorithm developed to address thermal inertia errors greatly improves the quality of salinity data, particularly when experiencing large temperature gradients. Finally, the stability of the RBR*argo*|deep6k CTD in the field is shown using the data from pilot deployments of RBR*argo*|deep6k CTD on Deep Argo floats.**

***Index Terms*—Deep Argo, CTD, thermal inertia, compressibility, stability**

I. Introduction

The Deep Argo program, a large-scale, long-term oceanography initiative, aims to collect high-quality data of pressure, temperature, and conductivity from the deepest parts of the world's oceans, reaching depths of up to 6000 dbar [16]. This ambitious goal necessitates the deployment of reliable instruments capable of providing accurate measurements at high pressures and over the lifetime of an Argo float (approximately 5 years). The aspirational accuracy specifications for Deep Argo pressure, temperature, and salinity measurements are ± 3 dbar, ± 0.001°C, and ± 0.002 PSS-78, respectively [13]. These requirements are in line with shipboard measurements from the Global Ocean Ship-Based Hydrographic Investigations Program (GOSHIP) [8].

As outlined in [13], the need for multiple CTD manufacturers in the Argo program is critical to avoid a single point of failure. Currently, two different CTDs are under trial for the Deep Argo program: the SBE61, manufactured by Sea-Bird Scientific, and the RBR*argo*|deep6k, manufactured by RBR. The accuracy specifications of the RBR*argo*|deep6k CTD provided by the manufacturer are $\pm$ 3 dbar, ± 0.002°C, and ± 0.003 mS/cm for pressure, temperature, and conductivity, respectively.

The primary technological challenge faced by the Deep Argo program is to maintain the level of accuracy of the CTDs established by the manufacturer in their calibration facilities throughout (1) the entire range of pressure experienced by a Deep Argo float (i.e. compressibility errors), (2) rapidly changing ocean conditions, such as temperature gradients (i.e. response time and thermal inertia errors), and (3) over the lifetime of a Deep Argo float (i.e. stability). In this work, we analyze the performance of the RBR*argo*|deep6k CTD over these three main aspects, combining laboratory and in-situ datasets.

II. Intrument design

The RBR*argo*|deep6k CTD comprises of three main sensors: a pressure sensor, a temperature sensor, and an inductive conductivity sensor. As for any inductive conductivity sensor, the conductivity cell comprises two toroidal coils, the primary and secondary coils, encased in a non-conductive material to withstand harsh marine environments (see Fig. 1). When an alternating current flows through the primary coil, it generates an alternating magnetic field in the ferrite that induces a current in the surrounding seawater, which is conductive due to its salinity. This induced current creates a secondary magnetic field that is detected by the secondary coil. The intensity of this induced current is directly proportional to the conductivity of the seawater, which can be converted to salinity. This non-contact method minimizes contamination and biofouling, ensuring reliable long-term salinity measurements crucial for oceanographic research and environmental monitoring.

III. theoretical framework

A. Static accuracy and compressibility errors

Static accuracy of the temperature, conductivity, and pressure from the RBR*argo*|deep6k is determined during the calibration process at RBR, and detailed on the calibration certificate provided by the manufacturer. The pressure channel is calibrated across the sensor's full range (i.e., 6000 dbar), and at different temperatures to characterize the temperature

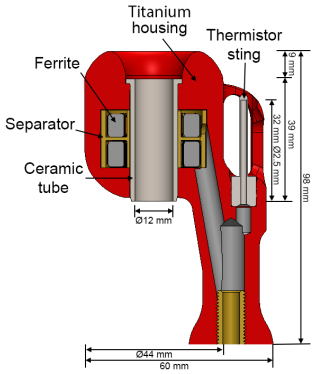

Fig. 1. Schematic of the RBR*argo*|deep6k

dependence of the pressure readings. Typically, temperature and conductivity sensors on CTDs are calibrated by the manufacturers at atmospheric pressure, across a range of temperature and salinity values. However, it is now well-shown that when pressure is applied to a conductivity cell (electrode-based or inductive), the cell tends to deform slightly and generates an error in the conductivity readings [2], [14]. Manufacturers have addressed this error in different ways: while some use data collected in-situ to establish a linear correction of conductivity with pressure across all instruments, RBR has developed an in-lab calibration process to characterize the pressure response of each individual RBR*argo*|deep6k CTD in controlled conditions. This process is described in [2] and validated for the 2000 dbar-rated RBR*argo*|2k. In this study, we seek to validate this laboratory process in the field to the maximum pressure rating of 6000 dbar.

B. Dynamic errors

Dynamic errors will affect the quality of the collected data when the measured conditions are changing more rapidly than the sensor can respond to. Dynamic errors affect CTD data independently of the CTD working principle (inductive or electrode-based), and is not restricted to CTD data and will affect any type of sensor. Dynamic errors generally stem from two different sources:

1) Inherent sensor response time: If environmental conditions vary faster than the instrument can respond, then the data will be affected by smearing and be smoothed. This can generate further errors when two measurements must be combined to obtain a derived quantity, like salinity. The conductivity sensor on the RBR*argo*|deep6k has an inherent response time that can be considered to be virtually instantaneous ($\sim$ 32 ms), while the thermistor has a time-response of 700 ms. Because conductivity and temperatrure measurements must be combined to compute salinity, the longer response-time of the thermistor relative to the conductivity cell will generate spurious data at sharp temperature interface, often referred to as "salinity spiking" [2], [3], [5] and can be addressed by shifting the temperature signal back in time to re-align conductivity and temperature measurements, thus minimizing the spiking. This lag is referred to as the "C-T lag" and is both characterized and independently-validated in this study for the RBR*argo*|deep6k.

2) Thermal inertia: As a CTD travels through a temperature gradient, heat is exchanged between the conductivity cell and the cell's boundary layer, which changes the temperature averaged over the conductivity measurement volume from that measured by the thermistor. Thus, the calculated salinity must use a temperature adjusted for the heat flux into the measurement volume. This is a well-known, but poorly constrained, error in CTD measurements generally, and is the focus of a research effort that has been ongoing for over three decades [2], [4], [6], [7], [9]–[11]. As described by [9], the thermal inertia errors will depend on the profiling speed as it controls boundary layer dynamics and the rate at which heat is exchanged between the conductivity cell and the surrounding water. The corrective algorithm used for the RBR*argo*|deep6k is identical to the one derived in [2] for it 2000 dbar-rated counterpart, and is based on the seminal work by [9] and [11]. In this study, we aim to (1) verify that the approach used for the RBR*argo*|2k is suitable for the RBR*argo*|deep6k and (2) derive the key coefficients required by the corrective algorithm.

Three coefficients are required to post-correct the conductivity data for thermal inertia errors (see [2]):

- The parameter $ctcoeff$, which is the factor that scales the temperature difference between the internal thermistor and the marine thermistor (see Fig. 1) to compute the estimated temperature anomaly generated by the cell's thermal inertia over relatively longer timescales O(100 s), using:

$$T_{long} = \text{ctcoeff}(Vp) \times (T_{cond} - T_{cor}) \tag{1}$$

  where T_{long} is the temperature anomaly in the sampled volume due to long-term thermal inertia, Vp is the water speed through the ceramic tube, T_{cond} is the internal temperature in the conductivity cell, and T_{cor} is the marine temperature adjusted for the C-T lag (see above).
- The parameters (α, τ), which drive the amplitude and the timescale of the Infinite Impulse Response (IIR) filter commonly used to correct thermal inertia errors over short timscales O(1s). This recursive filter is detailed in [9] and adjusted in [11], but relies on the following equation:

$$T_{short}(n) = -bT_{short}(n-1) + a[T_{cor}(n) - T_{cor}(n-1)] \tag{2}$$

  where T_{short} is the short-term temperature anomaly estimated by the filter, and n is the index for a discrete measurement. The two coefficients a and b are computed using

$$a = \frac{4 f_N \alpha \tau}{1 + 4 f_N \tau}$$
$$b = 1 - \frac{2a}{\alpha} \tag{3}$$

where f_N is the Nyquist frequency, and α and τ are empirically determined parameters (see section IV-B). The total estimated temperature of the sampled volume can be estimated by combining both T_{long} and T_{short} with the measured marine temperature:

$$T_{cell} = T_{cor} + T_{long} - T_{short} \tag{4}$$

where T_{cell} is the estimated temperature of the sampled volume, corrected for both long- and short-term thermal inertia, and is used to derive the corrected salinity.

C. Sensor stability

The long-term stability of the RBR*argo*|deep6k CTD is a characteristic that is particularly important to the Argo program, as the instrument cannot be recovered for re-calibration. It is thus essential that the conductivity cell remains stable not only through time, but also across many pressure cyclings. Because conductivity drift can be a function of either or both time and number of pressure cycles, it is challenging to test in the laboratory. The best solution is to deploy the instrument in the field and collect a dataset long enough that a trend can potentially be detected in the salinity measurements. A robust analytical tool was developed by [12] and refined in [1] to use climatological data at depth to detect potential drift in salinity measurements. This approach is taken to assess the stability of the conductivity cell measurements on the RBR*argo*|deep6k in Section V-D.

IV. Laboratory-based characterization

A. Static accuracy and compressibility errors

Similarly to the process described in [2], the RBR*argo*|deep6k CTD is pressurized in salt water to its maximum pressure rating to characterize the conductivity response to pressure in a controlled environment. The pressure tank used in this calibration process is chilled to 3.5°C to better represent the average deep ocean temperature. For practical reasons, the pressure tank cannot be directly filled with salt water as the pressure vessel would suffer corrosion and chemical reactions would potentially occur and affect the salinity of the water in the tank, which must be stable and well-measured. Instead, the RBR*argo*|deep6k is installed into a "saltbladder" which is an acrylic tube with a soft-lid, allowing the compression of the salt water inside the tube. A water pump is installed at the bottom of the tube to ensure that the water in the saltbladder is well-mixed and homogeneous.

Fig. 2 shows a pressure cycle during the compressibility calibration. Each pressure cycle includes 23 pressure plateaus to allow the temperature to equilibrate in the tank. Out of these 23 plateaus, 21 are used to derive a cubic polynomial model to remove the compressibility error in the conductivity measurements, using:

$$C_{meas} = \frac{C_{raw}}{1 + X2 \cdot P + X3 \cdot P^2 + X4 \cdot P^3} \tag{5}$$

where C_{raw} is the raw conductivity measured by the instrument, P is the sea pressure, ($X2$, $X3$, $X4$) is the set of compressibility correction coefficients, and C_{meas} is the compressibility-corrected conductivity.

Fig. 2 shows the salinity after being corrected using (5), effectively removing the impact of pressure on conductivity measurements, which now fits within the manufacturer's specifications across the whole range of pressure, and not only as atmospheric pressure.

B. Dynamic behavior and thermal inertia errors

Several conditions must be met to be able to confidently assess the dynamic response of a CTD, particularly on the conductivity measurements. First, a sharp and large temperature gradient must be experienced by the CTD. The sharpness of the gradient ensures that the measured response of the conductivity is not the result of a convoluted signal due to a slow changing gradient, while the amplitude of the temperature gradient guarantees a large signal-to-noise ratio. Second, the measured conditions around the CTD must be homogeneous and stable through timefollowing the temperature interface, for some time long enough to capture the slowest expected timescale. This is crucial to isolate the thermal inertia response of the conductivity cell, and properly resolve all the potential timescales driving the thermal adjustment of the conductivity cell. Finally, a constant water speed must be maintained to confidently characterize the dependence of the thermal inertia response as a function of the flow speed through the ceramic tube. A robust experimental setup was presented in [2], using a recirculating saltwater flume that meets all the requirements listed above. In this study, we use the same setup to characterize the thermal inertia response of the RBR*argo*|deep6k.

Following [2], the experimental protocol consists of cooling down the RBR*argo*|deep6k CTDs in an ice bath with a temperature below 3°C, to then swiftly plunge the CTD into the saltwater flume at a temperature over 15°C, where the CTD is left to equilibrate thermally. This creates a large step-change in the temperature experienced by the CTD. Fig. 3C shows an example time series of the salinity error resulting from the thermal inertia of the conductivity cell on the RBR*argo*|deep6k. The coefficient ctcoeff necessary to correct for the long-term thermal inertia (see (1)) is computed by fitting the derived T_{long} against the temperature difference between the marine temperature (T_{meas}) and the internal temperature measured in the conductivity cell (T_{cond}). The first 50 s of the plunge are ignored, as it is expected to be contaminated by the short-term thermal inertia of the conductivity cell. In fact, the expected timescale for the short-term thermal inertia is O(10 s). It is assumed that by ignoring the equivalent of five e-folding timescales, the remainder of

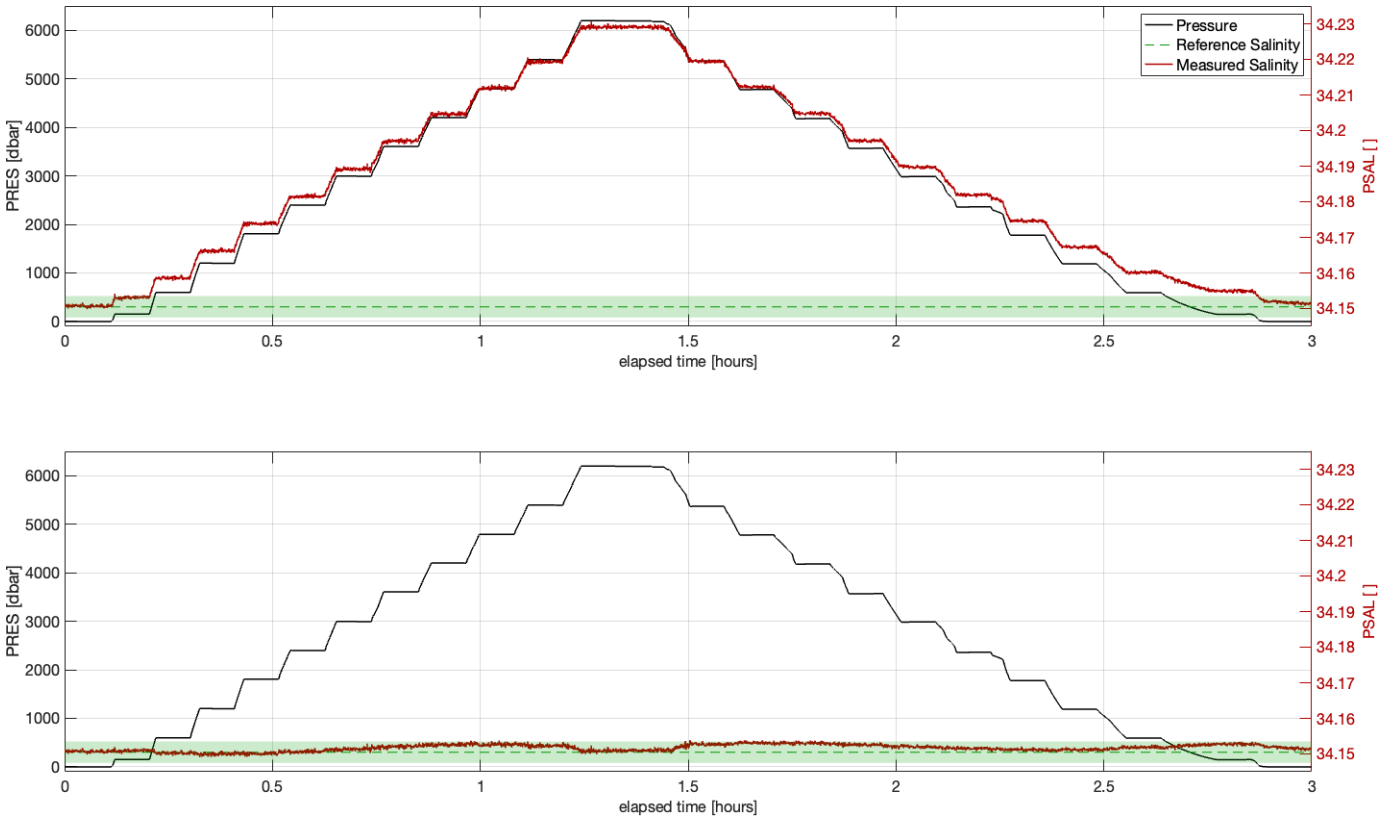

Fig. 2. Example of a time series of pressure (black) and salinity (red) [top] before and [bottom] after applying the compressibility calibration. The reference salinity of the saltbladder, along with its uncertainties, are indicated in green.

the salinity adjustment time series is dominated by the long-term thermal inertia adjustment only. This is confirmed by the linear behavior in T_{long} vs. $T_{cond} - T_{meas}$ after the first 50 s of the adjustment (Fig. 3A).

The two key coefficients necessary to correct for the short-term thermal inertia of the CTD, α and τ, are derived using the first 40 s of the plunge. The measured salinity is normalized to its initial and final values, thus varying between 0 and 1. The logarithm of this normalized salinity, SN, is then fitted with a linear model to derive the slope, which corresponds to the inverse of the adjustment timescale τ (Fig. 3B). Once tau is determined, the recursive filter introduced in (2) is applied using a range of α. For each value of α, the salinity root-mean-square-error (RMSE) is computed with respect to the reference. The α minimizing the RMSE is selected for this particular plunge (Fig. 3C). The time series of the salinity corrected for both long- and short-term thermal inertia errors is shown in (Fig. 3D), where most of the salinity error observed in the raw data is now corrected for.

This analysis was repeated over 32 plunges, over eight different water velocities ranging from 5 cm/s to 23 cm/s, and including three RBR*argo*|deep6k. Fig. 4 shows the observed relationships between the key coefficients (ctcoeff, α, and τ) as a function of the water speed. As in [9] and [2], a power law is fitted through the data to derive a model for each parameter, and each form factor of the RBR*argo*|deep6k CTD.

Each coefficient can then be modeled using, for the RBR*argo*|deep6k:

$$\begin{aligned} ctcoeff &= 0.09 \times V_p^{-1.17} \\ \tau &= 31.54 \times V_p^{-0.22} \\ \alpha &= 0.27 \times V_p^{-0.74} \end{aligned} \tag{6}$$

V. Field-based validation

A. Datasets

Two datasets are used to validate the laboratory-based results detailed above. In 2024, a research cruise called IN2024_T01 took place on board the R.V. *Investigator* and collected several profiles to 6000 dbar. The shipboard CTD rosette was equipped with a shipboard CTD (SBE9) and six RBR*argo*|deep6k. Water samples were collected in Niskin bottles to collect salinity samples that were analyzed onboard by a hydrochemist. As routinely done on a scientific research cruise, the salinity samples are used to calibrate the SBE9 by scaling the measured conductivity with a multiplicative factor. We apply this method to all seven CTDs mounted on the shipboard rosette for consistency.All CTDs are then aligned in time by using the "soaking" of the CTD rosette: for each profile, the rosette is first soaked in the ocean for 5 to 10 minutes to thermally equilibrate instruments mounted on the rosette. During this period, the pressure time series looks like a sinusoidal that reflects the ship's heaving due to surface

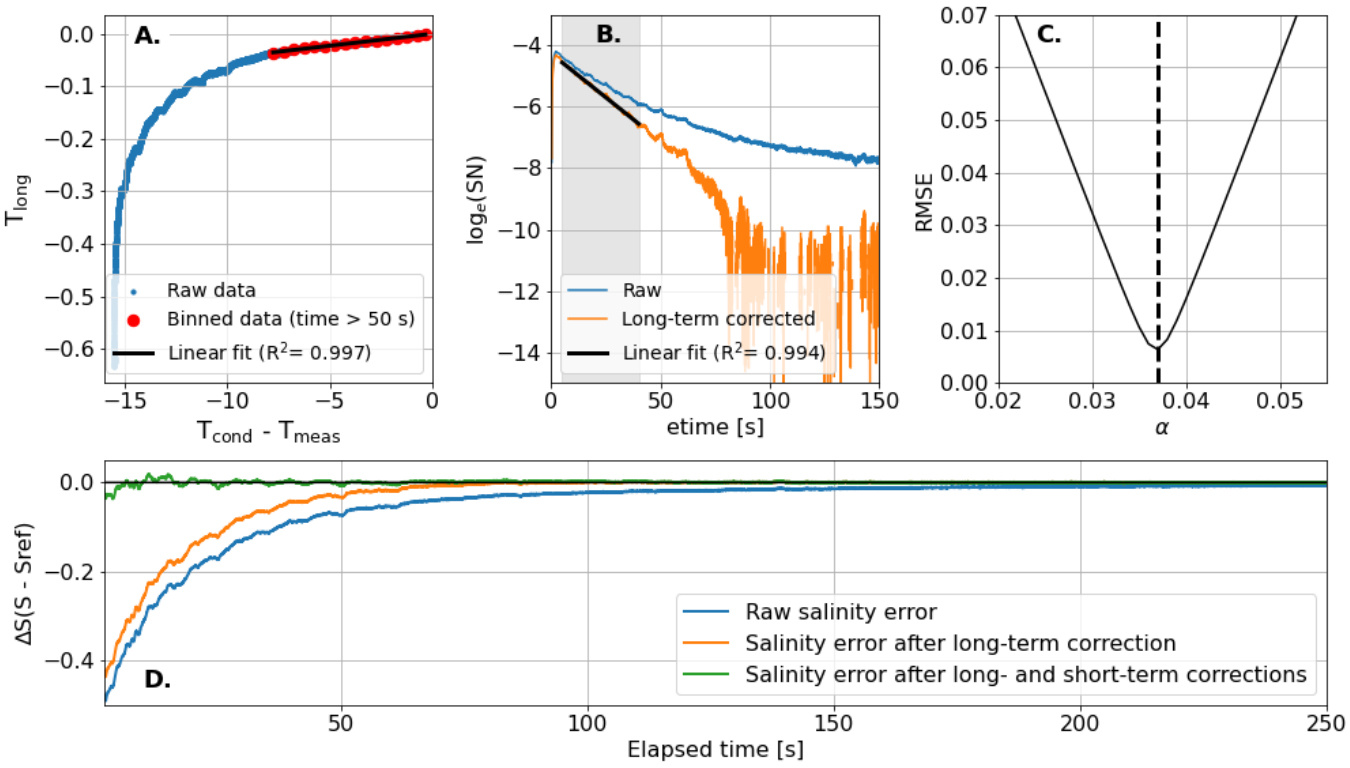

Fig. 3. Example of thermal inertia characterization of an RBR*argo*|deep6k in the saltwater flume, at 11.2 cm/s. **A.** Computed temperature anomaly as a function of the measured internal temperature at the ferrites (see Fig. 1). The linear fit applied to the data collected after 50 s is shown as a solid black line. **B.** Time series of the logarithm of the normalized salinity before (blue) and after (orange) applying the long-term correction algorithm given in (3). **C.** Root-mean-squared-error (RMSE) as a function of α. The selected α is shown with the dashed line. **D.** Salinity difference measured from the reference in the raw data (blue), after correcting for the long-term thermal inertia (orange), and after correcting for both the long- and short-term thermal inertia (green).

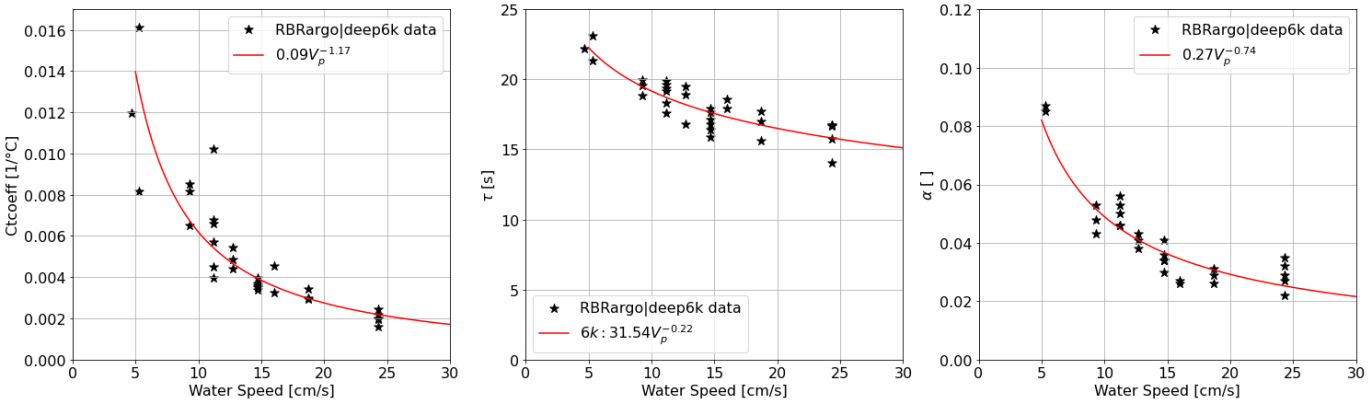

Fig. 4. [left] ctcoeff, [middle] τ, and [right] α measured during each plunge in the saltwater flume for [top] the RBR*argo*|deep6k. Power-law models for each parameter are shown in red.

waves. This signal is used to synchronize the clocks on each RBR*argo*|deep6k with the SBE9's clock. Comparing the CTDs in the time-space is necessary to evaluate the quality of the pressure data. It is also preferred when comparing temperature and conductivity measurements, as it avoids convoluting pressure measurement errors in the comparison.

The second dataset comes from a field experiment described in [15]. During this experiment, three Deep Argo floats capable of profiling to 4000 dbar were deployed with RBR*argo*|deep6k CTDs. For some profiles, those floats profiled through a sharp thermocline into the surface mixed layer, capturing ideal conditions to evaluate thermal inertia corrections for the RBR*argo*|deep6k in the field. One of these floats, WMO 2903882, profiled for 51 profiles over 479 days, forming an ideal dataset to evaluate the stability of the RBR*argo*|deep6k.

B. Static accuracy and compressibility errors

The static accuracy of the RBR*argo*|deep6k is evaluated by comparing pressure, temperature, and conductivity measurements to the shipboard CTD's (Fig. 5). The pressure accuracy of the RBR*argo*|deep6k falls within the expected accuracy specifications of the instrument with an average error of -0.05 $\pm$1.17 dbar. Only one profile exceeds the threshold of $\pm$3.15 dbar, to a maximum of +3.6 dbar. The temperature difference shows a very consistent behavior, with all units falling within the $\pm$0.003°C limits. The temperature difference are very consistent below 1000 dbar, and suggest a positive offset between 0.001°C and 0.003°C. The source of this offset is unknown and could be due equally to the SBE9's or the RBR*argo*|deep6k's accuracy. The noisier comparison in the upper 1000 dbar is most likely due to natural spatial variability in temperature, as the temperature gradients in that upper layer are larger, and the CTDs are not measuring the same water parcel. The comparison of conductivity measurements is shown in Fig. 5 and demonstrates that the compressibility errors detailed in Section III are indeed removed by the laboratory calibration, to the first order. This suggests that the second-degree polynomial used to correct the compressibility errors during calibration is an appropriate model to guarantee the manufacturer's conductivity specifications over the entire range of pressure. However, a structure can still be seen in the residuals consistent across profiles but different across the units tested in the field.

C. Dynamic behavior and thermal inertia errors

Dynamic errors are difficult to observe in situ. However, the conditions listed in IV-B are sometimes met in the ocean. In fact, when Argo floats profile upward through a warming temperature profile, with a sharp thermocline separating the warmer surface mixed layer from the colder ocean interior, thermal inertia errors can be seen as a fresh salinity error with an exponential adjustment as the float profiles through the homogeneous conditions of the surface mixed layer. It can also be seen as a light density error, often causing non-physical density inversions (Fig. 6). Examples of such density inversions are shown in Fig. 6 for three Argo floats equipped

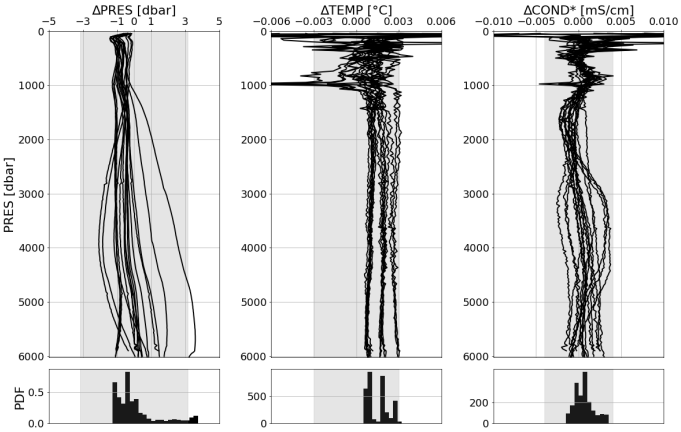

Fig. 5. Comparison between the six RBR*argo*|deep6k and the shipboard CTDs of pressure, temperature, and conductivity, for all profiles collected on the IN2024_T01 cruise. The bottom row shows the Probability Density Function (PDF) of the differences. The * in the conductivity panel indicates that the depth-average difference taken between 2000 and 6000 dbar was subtracted from the residuals. The grey-shading regions indicate the compounded uncertainties of the two instruments (SBE9 and RBR*argo*|deep6k) and are $\pm$3.15 dbar, $\pm$0.003 °C, and $\pm$0.004 for pressure, temperature, and conductivity, respectively.

with an RBR*argo*|deep6k. The raw data clearly shows an exponential adjustment as the float is profiling upward through the mixed layer. Correcting salinity data for thermal inertia errors using the relationships from (6) in (1) and (3), the corrected density profiles plotted in Fig. 6 no longer show density inversions at the base of the mixed layer, and are now more homogeneous throughout the mixed layer, down to the pycnocline. Fig. 6 supports the results obtained in the laboratory for correcting the thermal inertia errors on the RBR*argo*|deep6k.

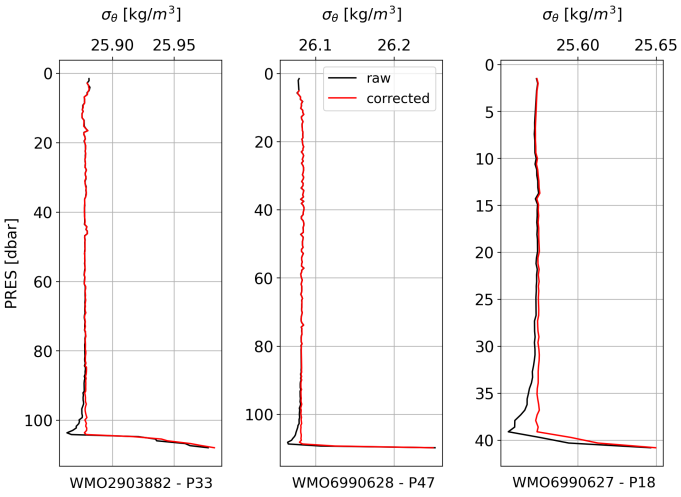

Fig. 6. Examples of density profiles measured by Deep Argo floats equipped with an RBR*argo*|deep6k CTD. Black lines show the raw data, while the red lines show the data corrected for thermal inertia errors. For each profile, the WMO number of the float is provided, along the profile number.

D. Sensor stability

In the context of profiling Argo floats, a robust and widely-used method has been developed by [12] and refined by [1]. This method, called the OWC, consists in comparing salinity measurements to a climatology along isotherms where the salinity variance is the smallest. It helps to determine if a conductivity sensor experiences drift, with increased confidence for longer time series. Similarly to [2], the OWC analysis is applied to all three Argo floats equipped with RBR*argo*|deep6k CTDs (see Section V-A. The time series of the normalized salinity anomalies derived from the OWC analysis are shown in Fig. 7 and reveal no statistically significant trends in the salinity accuracy from those three floats. WMO6990627 (19 profiles) presents a larger anomaly over its last three profiles, which would require more profiles to confirm a potential drifting behavior. WMO6990627 (49 profiles) includes a few outliers at profiles 44 and 48, but the observed variability in salinity anomalies remains within the uncertainties of the OWC analysis for the rest of the time series. WMO2903882 (76 profiles) remains stable throughout the time series with salinity anomalies within $\pm$ 0.10, well below the uncertainties of the OWC method. These results also confirm the findings in [15], where a similar stability analysis is conducted.

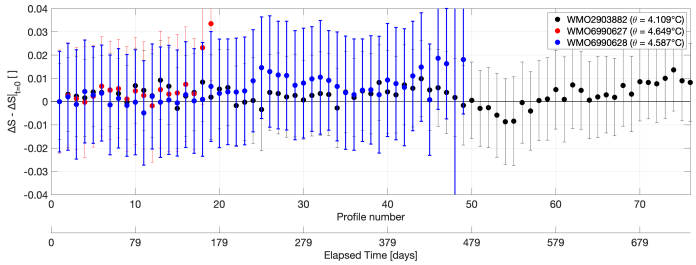

Fig. 7. OWC analysis [1], [12] on WMO2903882 (black), WMO6990627 (red), and WMO6990628 (blue). It shows the time series of the salinity anomaly observed by the float along a specific isotherm when compared to a climatology. The salinity anomaly is normalized to the first profile to better detect drift in the salinity measurements. The vertical error bars indicate the uncertainty associated with the comparison, as quantified by the OWC algorithm.

VI. Conclusions

Three aspects of the RBR*argo*|deep6k CTD were analyzed to characterize the performance of this CTD and evaluate its suitability for the Deep Argo mission. The compressibility errors affecting salinity data and generated by the impact of pressure on the conductivity measurements are characterized as part of the CTD calibration, similarly to the process outlined in [2] for the 2000 dbar-rated RBR*argo*|2k. The laboratory-based compressibility calibration can thus be extended to a 6000 dbar range while preserving the accuracy specifications of the CTD. The static accuracy of the RBR*argo*|deep6k for pressure, temperature, and conductivity measurements are shown to be valid over the entire 6000 dbar pressure range.

When oceanographic sensors are used in profiling applications, dynamic errors can affect the quality of the measurements and will impact all variables that present a temperature-dependence (e.g., oxygen, conductivity, pH). For CTDs, thermal errors particularly affect conductivity data, as the thermal inertia of the CTD when crossing temperature gradients can affect the temperature of the conductivity cell's measurement volume. Thermal inertia errors are a well-documented challenge in operational oceanography [2], [4], [6], [7], [9]–[11]. The relationship linking water speed through the conductivity cell and the three key parameters required to correct for thermal inertia errors using Eq. (1) and (2) are:
for the RBR*argo*|deep6k:

$$ctcoeff = 0.09 \times V_p^{-1.17}$$
$$\tau = 31.54 \times V_p^{-0.22}$$
$$\alpha = 0.27 \times V_p^{-0.74}$$

The corrective algorithm developed in the laboratory for thermal inertia errors on the RBR*argo*|deep6k seems to perform well in the field. The quality of the salinity data collected by three different Deep Argo floats is improved, as seen in Fig. 6. The artificial density inversions at the base of the mixed layer no longer persist when thermal inertia errors are corrected. Finally, the stability of the RBR*argo*|deep6k CTD is evaluated in the field using long time series collected on Deep Argo floats. No significant drift can be detected in the time series, including in the longest spanning over 470 days and 51 profiles.

Acknowledgements

The authors would like to thank the Commonwealth Scientific and Industrial Research Organisation (CSIRO) for funding the fieldwork onboard the RV *Investigator* and the technical crew onboard that supported the work. Thanks also extend to Virginie Thierry and Cecile Cabanes for sharing the Argo data to facilitate field-based validation of the work.

References

[1] Cécile Cabanes, Virginie Thierry, and Catherine Lagadec. Improvement of bias detection in argo float conductivity sensors and its application in the north atlantic. *Deep Sea Research Part I: Oceanographic Research Papers*, 114:128–136, 2016.

[2] M. Dever, B. Owens, C. Richards, S. Wijffels, A. Wong, I. Shkvorets, M. Halverson, and G. Johnson. Static and dynamic performance of the rbrargo3 ctd. *Journal of Atmospheric and Oceanic Technology*, 39(10):1525 – 1539, 2022.

[3] Mathieu Dever, Mara Freilich, J. Thomas Farrar, Benjamin Hodges, Tom Lanagan, Andrew J. Baron, and Amala Mahadevan. EcoCTD for Profiling Oceanic Physical–Biological Properties from an Underway Ship. *Journal of Atmospheric and Oceanic Technology*, 37(5):825–840, 2020.

[4] Mark Halverson, Eric Siegel, and Greg Johnson. Inductive-conductivity cell a primer on high accuracy ctd technology. *Sea Technology*, 61(2):24–27, 2020.

[5] E. P. W. Horne and J. M. Toole. Sensor Response Mismatches and Lag Correction Techniques for Temperature-Salinity Profilers. *Journal of Physical Oceanography*, 10(7):1122–1130, 1980.

[6] Gregory C. Johnson. Comments on "Corrections for Pumped SBE 41CP CTDs Determined from Stratified Tank Experiments". *Journal of Atmospheric and Oceanic Technology*, 37(2):351–355, 2020.

[7] Gregory C. Johnson, John M. Toole, and Nordeen G. Larson. Sensor Corrections for Sea-Bird SBE-41CP and SBE-41 CTDs. *Journal of Atmospheric and Oceanic Technology*, 24(6):1117–1130, 2007.

[8] Katsuro Katsumata, Sarah G. Purkey, Rebecca Cowley, Bernadette M. Sloyan, Stephen C. Diggs, Thomas S. Moore, Lynne D. Talley, and James H. Swift. Go-ship easy ocean: Gridded ship-based hydrographic section of temperature, salinity, and dissolved oxygen. *Scientific Data*, 9(1):103, 2022.

[9] Rolf G Lueck. Thermal Inertia of Conductivity Cells: Theory. *Journal of Atmospheric and Oceanic Technology*, 7(5):741–755, 1990.

[10] Kim I. Martini, David J. Murphy, Raymond W. Schmitt, and Nordeen G. Larson. Corrections for Pumped SBE 41CP CTDs Determined from Stratified Tank Experiments. *Journal of Atmospheric and Oceanic Technology*, 36(4):733–744, 2019.

[11] James Morison, Roger Andersen, Nordeen Larson, Eric D'Asaro, and Tim Boyd. The Correction for Thermal-Lag Effects in Sea-Bird CTD Data. *Journal of Atmospheric and Oceanic Technology*, 11(4):1151–1164, 1994.

[12] W.B. Owens and A.P.S. Wong. An improved calibration method for the drift of the conductivity sensor on autonomous ctd profiling floats by θ–s climatology. *Deep Sea Research Part I: Oceanographic Research Papers*, 56(3):450–457, 2009.

[13] Dean Roemmich, Matthew H. Alford, Hervé Claustre, Kenneth Johnson, Brian King, James Moum, Peter Oke, W. Brechner Owens, Sylvie Pouliquen, Sarah Purkey, Megan Scanderbeg, Toshio Suga, Susan Wijffels, Nathalie Zilberman, Dorothee Bakker, Molly Baringer, Mathieu Belbeoch, Henry C. Bittig, Emmanuel Boss, Paulo Calil, Fiona Carse, Thierry Carval, Fei Chai, Diarmuid Ó. Conchubhair, Fabrizio d'Ortenzio, Giorgio Dall'Olmo, Damien Desbruyeres, Katja Fennel, Ilker Fer, Raffaele Ferrari, Gael Forget, Howard Freeland, Tetsuichi Fujiki, Marion Gehlen, Blair Greenan, Robert Hallberg, Toshiyuki Hibiya, Shigeki Hosoda, Steven Jayne, Markus Jochum, Gregory C. Johnson, KiRyong Kang, Nicolas Kolodziejczyk, Arne Körtzinger, Pierre-Yves Le Traon, Yueng-Djern Lenn, Guillaume Maze, Kjell Arne Mork, Tamaryn Morris, Takeyoshi Nagai, Jonathan Nash, Alberto Naveira Garabato, Are Olsen, Rama Rao Pattabhi, Satya Prakash, Stephen Riser, Catherine Schmechtig, Claudia Schmid, Emily Shroyer, Andreas Sterl, Philip Sutton, Lynne Talley, Toste Tanhua, Virginie Thierry, Sandy Thomalla, John Toole, Ariel Troisi, Thomas W. Trull, Jon Turton, Pedro Joaquin Velez-Belchi, Waldemar Walczowski, Haili Wang, Rik Wanninkhof, Amy F. Waterhouse, Stephanie Waterman, Andrew Watson, Cara Wilson, Annie P. S. Wong, Jianping Xu, and Ichiro Yasuda. On the future of argo: A global, full-depth, multi-disciplinary array. *Frontiers in Marine Science*, 6, 2019.

[14] Sea-Bird Electronic, Inc. Compressibility compensations of sea-bird conductivity sensors. Technical Report Application note No. 10, Sea-Bird Electronic, Inc., 2013.

[15] Virginie Thierry, Cécile Cabanes, Martin Amice, Xavier André, Damien Desbruyères, Mathieu Dever, Cherif Diouf, Alberto Gonzalez, Guillaume Le Provost, Serge Le Reste, Corentin Renaut, and Pedro Velez-Belchi. Intercomparison of the SBE41CP, SBE61 and RBR*argo*|deep6k CTD probes for Deep-Argo application using three and two-headed Deep-Arvor floats. *Journal of Atmospheric and Oceanic Technology*, -, submitted.

[16] Nathalie V. Zilberman, Virginie Thierry, Brian King, Matthew Alford, Xavier André, Kevin Balem, Nathan Briggs, Zhaohui Chen, Cécile Cabanes, Laurent Coppola, Giorgio Dall'Olmo, Damien Desbruyères, Denise Fernandez, Annie Foppert, Wilford Gardner, Florent Gasparin, Bryan Hally, Shigeki Hosoda, Gregory C. Johnson, Taiyo Kobayashi, Arnaud Le Boyer, William Llovel, Peter Oke, Sarah Purkey, Elisabeth Remy, Dean Roemmich, Megan Scanderbeg, Philip Sutton, Kamila Walicka, Luke Wallace, and Esmee M. van Wijk. Observing the full ocean volume using deep argo floats. *Frontiers in Marine Science*, 10, 2023.